gastrointestinal disorders

MDPI

Article

Texture Analysis and Prediction of Response to Neoadjuvant Treatment in Patients with Locally Advanced Rectal Cancer

Ilaria Mariani [1], Cesare Maino [1,*], Teresa Paola Giandola [1], Paolo Niccolò Franco [1], Silvia Girolama Drago [1], Rocco Corso [1], Cammillo Talei Franzesi [1] and Davide Ippolito [1,2]

[1] Department of Diagnostic Radiology, IRCCS Fondazione San Gerardo dei Tintori, Via Pergolesi 33, 20900 Monza, Italy; i.mariani.dot@gmail.com (I.M.); teresagiandola1990@gmail.com (T.P.G.); francopaoloniccolo@gmail.com (P.N.F.); sgd.drago@gmail.com (S.G.D.); ctfdoc@gmail.com (C.T.F.); davide.ippolito@unimib.it (D.I.)

[2] School of Medicine, University of Milano Bicocca, Via Cadore 33, 20090 Monza, Italy

* Correspondence: mainocesare@gmail.com

Abstract: Background: The purpose of this study is to determine the relationship between the texture analysis extracted from preoperative rectal magnetic resonance (MR) studies and the response to neoadjuvant treatment. Materials and Methods: In total, 88 patients with rectal adenocarcinoma who underwent staging MR between 2017 and 2022 were retrospectively enrolled. After the completion of neoadjuvant treatment, they underwent surgical resection. The tumour regression grade (TRG) was collected. Patients with TRG 1–2 were classified as responders, while patients with TRG 3 to 5 were classified as non-responders. A texture analysis was conducted using LIFEx software (v 7.6.0), where T2-weighted MR sequences on oriented axial planes were uploaded, and a region of interest (ROI) was manually drawn on a single slice. Features with a Spearman correlation index > 0.5 have been discarded, and a LASSO feature selection has been applied. Selected features were trained using *bootstrapping*. Results: According to the TRG classes, 49 patients (55.8%) were considered responders, while 39 (44.2) were non-responders. Two features were associated with the responder class: *GLCM_Homogeneity* and *Discretized Histo Entropy log 2*. Regarding *GLCM_Homogeneity*, the area under the receiver operating characteristic curve (AUC), sensitivity, and specificity were 0.779 (95% CIs = 0.771–0.816), 86% (80–90), and 67% (60–71). Regarding *Discretized Histo Entropy log 2*, we found 0.775 AUC (0.700–0.801), 80% sensitivity (74–83), and 63% specificity (58–69). Combining both radiomics features the radiomics signature diagnostic accuracy increased (AUC = 0.844). Finally, the AUC of 1000 bootstraps were 0.810. Conclusions: Texture analysis can be considered an advanced tool for determining a possible correlation between pre-surgical MR data and the response to neoadjuvant therapy.

Keywords: magnetic resonance imaging; neoplasms; rectal; radiomics

Citation: Mariani, I.; Maino, C.; Giandola, T.P.; Franco, P.N.; Drago, S.G.; Corso, R.; Talei Franzesi, C.; Ippolito, D. Texture Analysis and Prediction of Response to Neoadjuvant Treatment in Patients with Locally Advanced Rectal Cancer. *Gastrointest. Disord.* **2024**, *6*, 858–870. https://doi.org/10.3390/gidisord6040060

Academic Editor: Tamara Čačev

Received: 25 September 2024
Revised: 15 October 2024
Accepted: 22 October 2024
Published: 28 October 2024

1. Introduction

Rectal cancer, aside from being the third cause of oncologic-disease-related death worldwide, is a significant cause of disability due to surgical complications and faecal incontinence. In this panorama, the *watch and wait* (W&W) approach, first theorised by the Habr-Gama [1] study group in 2004, raised much interest among the medical community [2], as it allows patients responding to neoadjuvant treatment to avoid surgery without a significant prognosis impairment [1,3–5] and undergoing periodic follow-up instead, with the possibility of endoscopic or surgical treatment if relapsing. Even if with promising results, it is still not equally applied among different countries. For example, while the National Comprehensive Cancer Network (NCCN) includes the W&W in its guidelines as a possible treatment strategy, the European Society for Medical Oncology (ESMO) guidelines only consider the W&W approach in the context of clinical trials [6–8]; the difference could

be explained by the lack of objective data to reliably assess the response on restaging magnetic resonance (MR), and the difficulty in allocating enough resources to instate periodic follow-ups, thus paving the way to uncertainty and relapse. Moreover, there is still a wide variability concerning the follow-up strategies in conservatively treated patients (e.g., the NCCN suggests performing a sigmoidoscopy and digital rectal examination every three months for the first two years after diagnosis, and MR every six months): the uncertainty regarding the procedures and timing for follow-up makes it critical to allocate healthcare resources to properly manage the risk of relapse, especially considering how differently organised any country's healthcare system is. The main reason for such a variability is the absence of objective and highly reproducible instruments to assess the pre-surgical response, which could enable all radiologists to evaluate the response after neoadjuvant treatment confidently. The response to neoadjuvant treatment is currently determined on restaging MR, where normal rectal wall stratification and the absence of areas of restriction to diffusion or a high T2-signal are indicators of absent disease. However, it can be difficult to detect these features, as chemoradiotherapy may cause inflammatory changes that could be mistaken for persistent disease (and vice versa), as well as mucinous degeneration. Moreover, restaging rectal cancer MR can be difficult and requires an expertise that not many centres could guarantee: that is why the pressure of finding objective parameters to rely on for determining the response is high on the scientific community. While most studies today have focused on extracting a threshold value from diffusion-weighted images (DWIs) to discriminate between responders and non-responders [9–15], radiomics is now taking the scene. It assumes that images are information, and, thus, the distribution of grey levels inside an image reflects the underlying histological structures of a specific tissue [16–18]. Through texture analysis, it is possible to obtain quantitative information regarding the distribution of signal intensities inside a desired structure, thus reflecting its underlying architecture and organisation. Many authors explored the field and focused explicitly on MR sequences such as T2-weighted (T2w), DWIs, and dynamic contrast-enhanced (DCE) sequences [16,19–21]. However, none of the above authors reached the point of designing a reproducible and solid algorithm to, indeed, discriminate between the two categories (responders vs non-responders), mainly due to the intrinsic complexity of the radiomic and texture analysis process and the risk of selecting over-fitting features [22–25]. On these bases, our retrospective study aims to test whether radiomic features can reliably distinguish between responders and non-responders according to Mandard's Tumour Regression Grade (TRG).

2. Materials and Methods

2.1. Patient Selection

We retrospectively collected patients from 2017 to 2022 who were diagnosed with rectal cancer after colonoscopy and biopsy, and they were then selected according to inclusion and exclusion criteria. Inclusion criteria were: (1) biopsy-proven rectal adenocarcinoma, and (2) staging MR examination showing a locally advanced rectal cancer before starting chemoradiation therapy (CRT).

Exclusion criteria were as follows: (1) anal involvement, (2) distant metastases at diagnosis, (3) MR examination obtained in other centres, (4) low-quality MR examination (e.g., including metal or movement artifacts), (5) patients unfit for CRT or surgery, (6) CRT or surgery performed in other centres, and (7) lack of histological diagnosis.

Flow chart in Figure 1 summarises the selection process.

All patients underwent neoadjuvant treatment via the FOLFOX/FOLFIRI scheme combined with short-course radiotherapy according to the ESMO guidelines. Treatment duration varied from two to three months. Restaging MR was performed at ten weeks after completion of chemoradiation treatment.

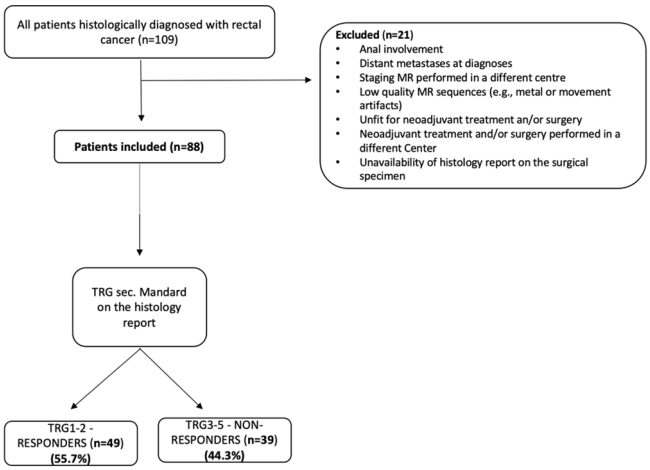

Figure 1. Flow chart of the study.

Surgery was performed between 1 to 8 weeks after restaging MR: it consisted of either trans-mesorectal excision (TME) or rectal anterior resection (RAR) with subsequent colostomy, following multidisciplinary discussion (including at least one radiologist, one surgeon, one oncologist, and one pathologist).

2.2. MR Technique and Patients' Preparation

All patients underwent MR on a 1.5T magnet (Philips Ingenia, Netherlands) with 16 high-resolution body array coil and the same study protocol, whose core are T2W sequences acquired on three planes (sagittal, oblique axial, and oblique coronal) following the ESGAR Consensus Panel [1].

The protocol included DWI sequences with four *b* values (*b*0, *b*50, *b*800, *and b*1000), according to current literature and clinical practice [26]. The MR scanner automatically created the corresponding apparent diffusion coefficient (ADC) map. Table 1 summarises the MR protocol used in our institution.

Table 1. MR protocol for rectal cancer.

	T1W Axial	T2W Axial	T2W Sagittal	T2W Axial Oblique	T2W Coronal Oblique	DWI
Slice thickness	5 mm	5 mm	3.5 mm	3 mm	3 mm	4 mm
Repetition time (ms)	688	4080	3654	7074	3539	3718
Echo time (ms)	14	100	100	85	85	81
Flip angle	90°	90°	90°	90°	90°	90°
FOV AP (mm)	440	440	200	200	180	375
rFOV (mm)	440	440	200	200	180	312
Acquisition matrix	324 × 253	292 × 292	252 × 198	336 × 251	256 × 182	124 × 105
NSA	1	2	2	2	2	2
Acquisition time (min)	1.56	1.30	4.38	5.18	3.32	4

All patients underwent bowel preparation and cleansing the day before the examination. Particularly, patients were instructed to follow a clear liquid diet, without eating any solid foods and only drinking clear liquids one full day before the MR. Few minutes before performing the examination, a rectal enema was performed, to obtain a clearance of the rectal lumen. Before performing the examination, the rectum was filled with 100 mL of warm ultrasound gel, while no spasmolytic drugs were routinely employed.

2.3. ROI Delineation

MR images were collected for any patient via DICOM file format and uploaded in a free-source radiomic software (LiFEx—v7.6.0) [27], which satisfies the Image Biomarker Standardisation Initiative (IBSI)'s requirements. The software automatically displayed all the MR sequences, among which a single radiologist (with four years of experience in pelvic MR) selected T2w paraxial sequences.

Before starting the segmentation process, a reading session with a more experienced radiologist (10 years of experience in radiomics and abdominal imaging) was performed. MR data used in the reading session, composed of 10 external examples with typical imaging features, were similar to the final cohort and were excluded from the analysis.

The chosen sequence was then exploited on the monitor, and the radiologist identified the slice where the tumour was most extensive. Then, the radiologist delineated the lesion by manually drawing a 2D region of interest (ROI) after selecting the number of bins. As suggested by the LiFEx user manual, we used a fixed bin width equal to 128 to perform the signal intensity discretisation and obtain isotropic pixels via spatial resampling.

Only tumoral tissue was selected during segmentation, avoiding the healthy rectal wall, mesorectal fat, and nodes near the rectal lesion. After completing the manual delineation, the software automatically derived the texture-based features for each patient, along with a histogram representing the distribution of pixels' intensities within the selected plane (Figure 2). The histogram was mainly considered as an indicator of the delineation's accuracy and reliability of signal intensities' "normal" distribution inside the selected ROI.

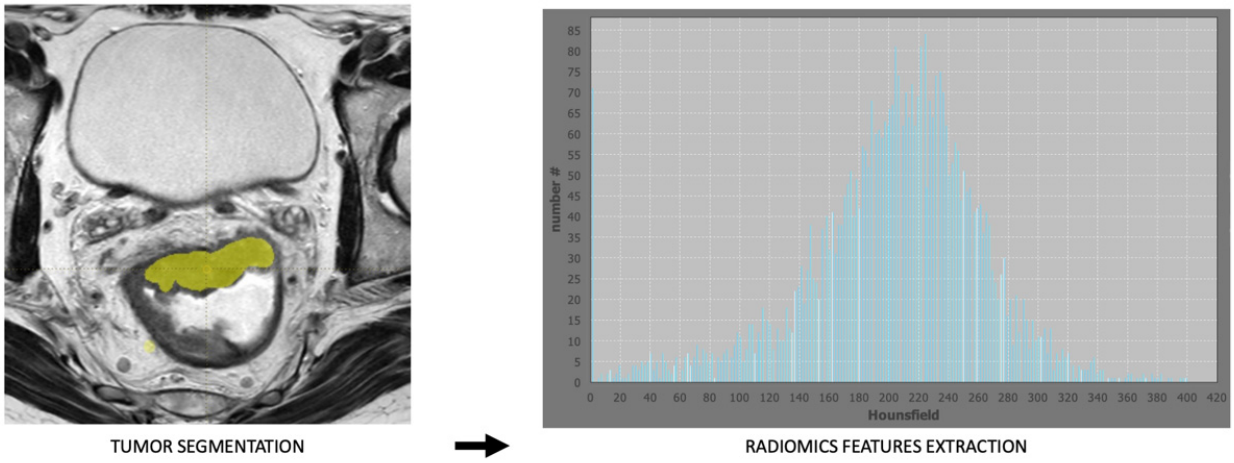

Figure 2. Radiomic features' extraction process. On the left, the yellow section depicts the manually delineated ROI, which is carefully selected to avoid the inclusion of a healthy wall or surrounding adipose tissue. On the right panel, the histogram represents the distribution of pixels' signal intensities, which the software automatically generates after ROI's delineation. After this process, the radiomics feature extraction was generated by the software.

2.4. Texture Analysis

The LiFEx software automatically extracted 452 features per ROI, which we selected via the LASSO regression test to avoid redundancy and overfitting. The obtained features were distinguished among first-, second-, and third-order features: these mathematical features picture the distribution of signal intensities inside an ROI and, hypothetically, the histological organisation of the underlying tissues. First-order features are an "absolute" parameter representing purely the distribution of signal intensities (also called "histogram-based" features). At the same time, second-order features highlight the existing relationship between the intensity levels of neighbouring pixels or groups of pixels within the segmented lesion (also called "texture-based features"). Finally, third-order features allow us, via the application of mathematical computational models, to extract information regarding the appearance of the whole segmented region.

2.5. Pathological Analysis

For all selected patients, the histology report included the Mandard's TRG, which describes the amount of residual tumoral cells inside the surgical specimen and, thus, quantifies response to neoadjuvant treatment. It distinguishes five classes: TRG1 includes patients for whom no residual cancerous cells are detected, TRG2 defines patients for whom there is no significant residual disease (or rather with a few cancerous cells outnumbered by fibrotic tissue), TRG3 identifies cases of dubious response (where the amount of tumoral cells significantly increases, but still does not overcome the fibrotic tissue), TRG4 identifies situations where tumoral cells prevail over normal or fibrotic tissue, and TRG5 describes those patients who did not respond at all and where there was no significant reduction in number of cancerous tissue.

2.6. Statistical Analysis

To evaluate textural features' performance, we divided our population into two subcategories, according to the histological TRG: TRG1–2 patients were considered among responders, while TRG3–5 patients were considered non-responders.

A nonparametric measure used to describe the relationship between two variables is the Spearman's correlation coefficient: it captures nonlinear interactions by comparing the statistical dependency of the variable rank. Strong correlations were defined as those with a 0.9 or higher. Features that showed a very high correlation with a single traditional metric were eliminated from the study since they were deemed redundant.

The most helpful predictive features were then found using the logistic regression model with the least absolute shrinkage and selection operator (LASSO). LASSO is a regression analysis technique that uses penalised estimation functions to select and regularise features in order to increase prediction accuracy.

After the LASSO regression test allowed the elimination of the redundant data and the harmonising of the remaining ones, a correlation test was run to determine which texture sub-features retain some correlation with the histological response to treatment. We then performed bootstrapping with 1000 iterations.

After selecting radiomics features associated with the responders and non-responders groups, median values of each feature were used to compute diagnostic values [sensitivity, specificity, negative predictive, and positive predictive values (NPV and PPV, respectively), and accuracy] using crosstabs.

All tests were two-sided, and the p-value ≤ 0.05 was considered statistically significant. All the statistical analyses were performed using IBM SPSS 28.0 (SPSS Incorporated, Chicago, IL, USA).

3. Results

After selection via the aforementioned criteria, we obtained a final cohort of 88 patients (51 males and 37 females; the median age at diagnosis: 66.8 years). They were further subclassified according to their respective TRG's status as non-responders (39, 55.7%) and responders (49, 44.3%).

3.1. Clinical Data

A total of 55.7% showed a histological response to neoadjuvant treatment, while the remaining 44.3% was considered as non-responders. After collecting TRGs, we also followed our patients during their follow-up: 58 (65.9%) did not show signs of recurrent disease at the 5-year follow-up. Six patients (6.8%) were lost at follow-up; we could not include them in our observation. The remaining 24 cases (27.2%) underwent disease recurrence during the follow-up period, mainly due to the development of metastatic disease (in the nodes and liver) or the persistence of a residual tumour on the surgical bed (R1 at histology report).

3.2. Texture Analysis

After applying the LASSO regression test, 67 features per patient were obtained.

Discretized Histo Entropy log 2 was the only histogram-based feature capable of discrimination between responders and non-responders, with an eight-times difference between the two subpopulations (B = 8.331, 95%CIs 7.691–10.428, p = 0.003). *Histo-Entropy_log2* showed a reasonably good performance in discriminating between responders vs non-responders, with an 80% sensitivity (95%CIs = 74–83%), 63% specificity (95%CIs = 58–69%), 77% and 82% PPV and NPV, respectively, and 77.5% accuracy (95%CIs = 70–80.1%). Table 2 summarises the LASSO regression analysis computed for first-order texture features.

Table 2. First-order features selected after LASSO regression test. Among all the features extracted, only Histo_Entropy_log2 resulted in a significant capability of differentiation between responder and non-responder. For the LASSO regression, the reference was the responder group.

Feature	**Corrected B**	**95%CIs**		***p*-Value**
		min	**max**	
CONVENTIONAL_HUmin	3.036	0.668	8.501	0.223
CONVENTIONAL_HUmean	2.878	2.310	10.484	0.374
CONVENTIONAL_HUstd	7.517	5.739	13.945	0.722
CONVENTIONAL_HUmax	8.992	7.313	11.187	0.804
CONVENTIONAL_HUQ1	5.477	4.151	8.974	0.719
CONVENTIONAL_HUQ2	1.364	−0.108	2.830	0.321
CONVENTIONAL_HUQ3	9.712	9.231	18.995	0.737
CONVENTIONAL_HUSkewness	0.820	0.189	9.278	0.614
CONVENTIONAL_HUKurtosis	0.188	−1.017	8.645	0.505
CONVENTIONAL_HUExcessKurtosis	0.614	−0.162	9.541	0.517
CONVENTIONAL_RIM_HUmin	4.196	1.341	12.626	0.243
CONVENTIONAL_RIM_HUmean	1.535	−0.629	10.570	0.487
CONVENTIONAL_RIM_HUstdev	0.806	−0.240	3.904	0.118
CONVENTIONAL_RIM_HUmax	6.472	4.698	13.486	0.150
CONVENTIONAL_RIM_HUVolume	1.388	−1.068	2.757	0.624
CONVENTIONAL_RIM_HUsum	2.821	2.188	8.599	0.289
DISCRETIZED_HUmin	8.502	5.741	11.940	0.218
DISCRETIZED_HUmean	9.902	9.656	12.522	0.422
DISCRETIZED_HUstd	2.017	−0.579	2.401	0.531
DISCRETIZED_HUmax	8.695	8.629	15.429	0.564
DISCRETIZED_HUQ1	7.514	7.486	15.391	0.804
DISCRETIZED_HUQ2	4.075	3.359	5.998	0.833
DISCRETIZED_HUQ3	3.725	3.075	6.441	0.589
DISCRETIZED_HUSkewness	8.166	5.583	12.949	0.523

Table 2. *Cont.*

Feature	Corrected B	95%CIs		*p*-Value
		min	max	
DISCRETIZED_HUKurtosis	6.760	4.352	16.595	0.700
DISCRETIZED_HUExcessKurtosis	6.552	3.918	12.059	0.691
DISCRETIZED_HISTO_Entropy_log10	0.362	−1.382	6.493	0.638
DISCRETIZED_HISTO_Entropy_log2	8.331	7.691	10.428	0.003
DISCRETIZED_HISTO_Energy [=Uniformity]	2.476	2.443	2.938	0.458
DISCRETIZED_AUC_CSH	2.439	1.332	11.129	0.306
DISCRETIZED_RIM_HUmin	0.106	−1.466	4.483	0.237
DISCRETIZED_RIM_HUmean	0.384	0.268	3.570	0.197
DISCRETIZED_RIM_HUstdev	4.724	2.375	14.204	0.736
DISCRETIZED_RIM_HUmax	6.381	3.834	15.313	0.093
DISCRETIZED_RIM_HUsum	9.291	6.646	12.168	0.274

GLCM_Homogeneity was the only significant feature helping distinguish between responders and non-responders, with a nine-times difference between the median values of the two subpopulations (B = 9.072; 95%CIs = 7.946–18.357, p = 0.004). *GLCM_Homogeneity* showed a reasonably good performance in discriminating between responders vs non-responders, with an 86% sensitivity (95%CIs = 80–90%), 67% specificity (95%CIs = 60–71%), 81% and 88% PPV and NPV, respectively, and 77.9% accuracy (95%CIs = 77.1–81.6%). Table 3 summarises the LASSO regression analysis computed for second-order texture features. Figure 3 reported an example of responder and non-responder patients.

Table 3. Second-order radiomic features selected after LASSO regression test. Among all the features, GLCM_Homogeneity was the only one with a significant capability of discrimination between our two target groups. For the LASSO regression, the reference was the responder group.

Feature	Corrected B	95%CIs		*p*-Value
		min	max	
GLCM_Homogeneity [=InverseDifference]	9.072	7.946	18.357	0.004
GLCM_Energy [=AngularSecondMoment]	0.998	−0.288	5.901	0.157
GLCM_Contrast [=Variance]	6.626	5.163	13.350	0.839
GLCM_Correlation	8.534	7.282	8.676	0.345
GLCM_Entropy_log10	2.059	1.633	7.999	0.512
GLCM_Entropy_log2 [=JointEntropy]	4.273	3.064	12.434	0.196
GLCM_Dissimilarity	3.204	2.095	9.535	0.743
GLRLM_SRE	0.615	−0.237	4.620	0.702
GLRLM_LRE	5.991	4.491	6.086	0.158
GLRLM_LGRE	4.996	2.451	7.431	0.864

Table 3. *Cont.*

Feature	Corrected B	95%CIs		*p*-Value
		min	max	
GLRLM_HGRE	7.530	7.448	13.936	0.790
GLRLM_SRLGE	2.308	0.622	12.014	0.781
GLRLM_SRHGE	4.137	1.385	12.582	0.570
GLRLM_LRLGE	6.632	5.665	8.221	0.503
GLRLM_LRHGE	5.604	3.657	14.327	0.123
GLRLM_GLNU	3.500	3.291	10.624	0.365
GLRLM_RLNU	8.220	7.394	16.867	0.363
GLRLM_RP	3.720	1.268	12.588	0.300
NGLDM_Coarseness	6.948	4.251	10.424	0.800
NGLDM_Contrast	5.190	3.675	12.618	0.526
NGLDM_Busyness	5.084	2.787	6.938	0.557
GLZLM_SZE	8.786	6.138	15.255	0.749
GLZLM_LZE	2.380	0.877	8.874	0.851
GLZLM_LGZE	0.231	0.134	9.652	0.061
GLZLM_HGZE	0.028	−0.204	1.988	0.802
GLZLM_SZLGE	2.404	0.899	8.676	0.422
GLZLM_SZHGE	6.937	6.366	15.250	0.851
GLZLM_LZLGE	6.041	3.873	8.421	0.784
GLZLM_LZHGE	0.314	−0.525	9.400	0.543
GLZLM_GLNU	0.271	−1.708	3.410	0.213
GLZLM_ZLNU	6.650	4.799	12.793	0.316
GLZLM_ZP	2.594	1.510	11.939	0.498

Combining both radiomics features increased the radiomics signature diagnostic accuracy to 84.4% (95%CIs = 82.2–86.7%). Finally, the accuracy of 1000 bootstraps was 81% (95%CIs = 80.1–83.7%) (Table 4).

Table 4. Performance of the two selected textural features. Both had a satisfactory performance.

	Histo_Entropy_log2	GLCM_Homogeneity
Sensitivity (95%CIs)	80% (74–83%)	86% (80–90%)
Specificity (95%CIs)	63% (58–69%)	67% (60–71%)
PPV (95%CIs)	77% (80–81%)	81% (76–84%)
NPV (95%CIs)	82% (80–85%)	88% (84–90%)
Accuracy (95%CIs)	77.5% (70–80.1%)	77.9% (77.1–81.6%)

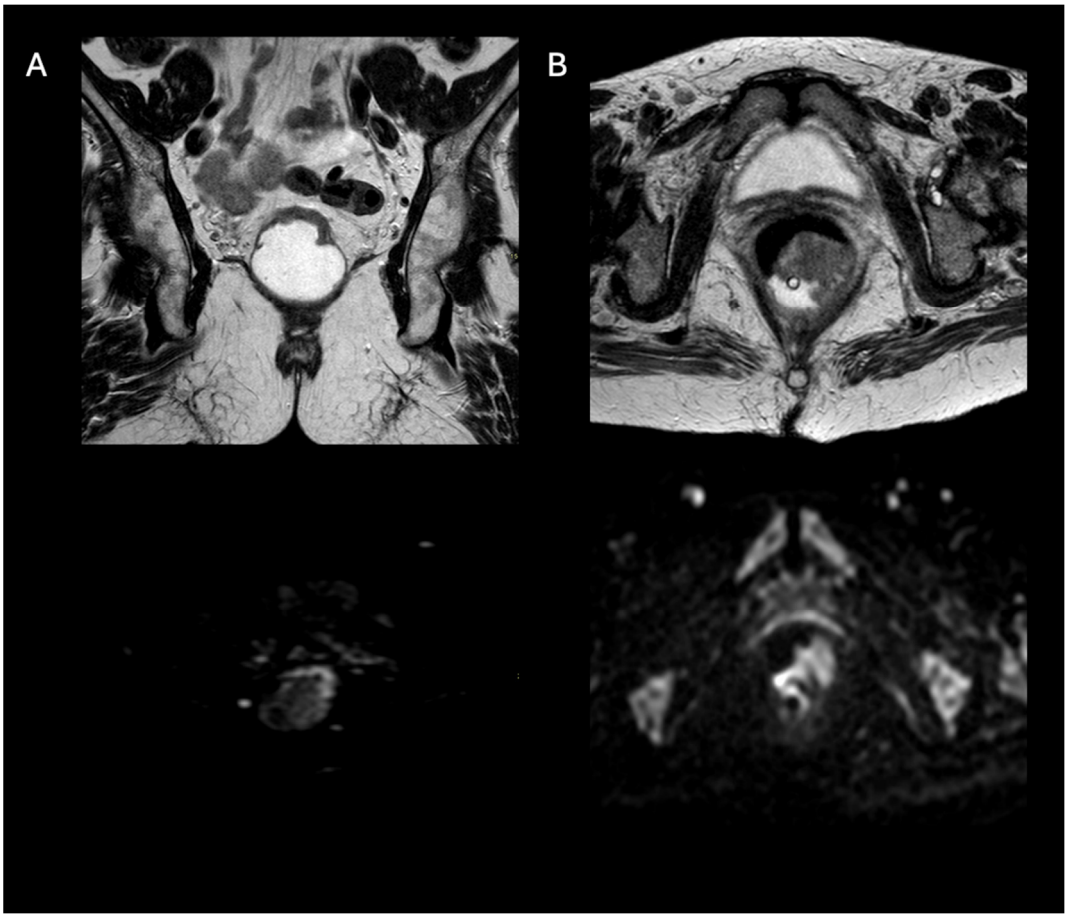

Figure 3. Two examples of patients who underwent MR were considered responders ((**A**)—TRG 1) and non-responders ((**B**)—TRG 4). The conventional evaluation of T2w sequences (first line) and DWI (second line) cannot help discriminate between significant differences in two patients. However, by computing texture analysis of the rectal tissue, it is possible to obtain quantitative data regarding them. Notably, the DISCRETIZED_Histo_Entropy_log2 values were 8.001 and 9.798, while GLCM_Homogeneity values were 15.879 and 7.771 for the responder and non-responder patients, respectively.

4. Discussion

According to our results, texture analysis has the potential to pre-operatively discriminate between responders and non-responders via two features showing a statistically significant difference among the subpopulation into which we categorised patients. *HISTO_Entropy_Log2* tends to be eight times higher in the non-responders, while *GLCM_Homogeneity* is nine times higher in the responders' subpopulation.

Texture analysis is a promising tool in artificial intelligence and is currently being explored for its capabilities in creating a personalised treatment protocol for many oncologic diseases [25,28], such as rectal cancer [20,21,29,30].

There is widespread interest in texture analysis due to its implications for treatment: as Staal et al. [31] summarised in a recent review, T2w-image-based models yield great potential in predicting the response to treatment (AUC between 63% and 79%), and entropy was the most reproducible feature among different studies, being higher in patients not responding to treatment. Although radiomic feature extraction is challenging due to its dependency on the acquisition protocol and on the normalisation, interpolation, and resampling process, which strongly depend on the signal intensity [32–34], it could potentially avert controversies during the reading of restaging images, where the discrimination between inflammation and residual disease is critical. As Achilli et al. highlighted [35], the

MR-based TRG modestly agrees with the pTRG and is biased by the low sensitivity and low positive predictive value. Not even functional imaging is discriminative, due to the limitations in terms of vendors' algorithms (e.g., diffusion-weighted imaging and ADC—apparent diffusion coefficient—mapping) and reduced availability (e.g., fusion imaging, such as PET/MR) [36]. Considering this background, the scientific community shall be encouraged to conduct research about strategies for implementing radiomics' reproducibility and applicability in daily life, not only by defining rapid and secure delineation strategies, but also by determining which features best serve the purpose.

Among the data we analysed, *HISTO_Entropy_log2* and GLCM_*Homogeneity* were the most significant textural features: according to the IBSI standard [37], grey-level co-occurrence matrix (GLCM) features fit better in a situation in which a high number of grey levels are analysed (as it is in our case); they belong to the "second-order features" group and depict the relationship existing between signal intensities in neighbouring pixels, thus reflecting the tissues' heterogeneity (or, as for GLCM_*Homogeneity*, their similitude in architecture); GLCM features specifically describe the frequency of occurrence of two intensity levels in neighbouring pixels or voxels within a specific distance along a fixed direction. On the other hand, *HISTO_Entropy_log2* belongs to the "first-order features" class and it is a statistical measure of the randomness of grey levels' distribution inside an ROI, in absolute terms.

Interestingly, as Robins et al. [38] highlighted, entropy and homogeneity are among the most stable radiomic features, which aligns with our results for responders and non-responders. Based on similar findings from other authors, we are optimistic that our results could be replicated in different patient cohorts. From an empirical perspective, we compared the *HISTO_Entropy_log2* and *GLCM_Homogeneity* values of a responder and a non-responder and found that *GLCM_Homogeneity* is tendentially higher in patients responding to treatment, while *HISTO_Entropy_log2* tends to be lower in patients not responding to treatment. Our findings are aligned with the definition of HISTO_*Entropy_log2* and GLCM_*Homogeneity* themselves, so they come as no surprise and are adherent to the histology findings.

To test and strengthen our results, we aim to walk a few more steps: first, we would like to combine the analysis of "morphological" T2w sequences with functional DWI sequences and create an algorithm that integrates imaging and clinical data (e.g., age at diagnosis, presence of extramural vascular invasion—EMVI—or nodal involvement, concurrent diseases, etc.), which other authors [39] have proven to perform well, also significantly improving inexperienced readers' performance.

Some limitations should be disclosed. Firstly, our cohort was relatively small, considering that radiomics studies should be as wide as possible. Furthermore, we are aware that one of the main limitations of our study is how we performed the segmentation process. Firstly, we used a 2D segmentation process instead of a 3D process, and we only considered the paraxial plane when delineating the ROI, thus opening up the possibility of losing some information. Implementing sequences in the sagittal and para-coronal planes could help obtain a complete overview of the tumour. We also manually selected the ROI, which many authors [40–42] recognise as a scarcely reproducible approach that is prone to error (especially if carried out by an inexperienced operator); thus, semi-automatic or deep-learning-based methods could be considered to reduce variability. In addition to that, radiomics application requires a great, cumulative effort as it is deemed by the complexity of the statistical analysis to be performed to delineate a reliable model, so that the efforts should be aimed also to simplify the selection process to the core, in order to make any potentially "universal" radiomics model friendly to the daily work-process in Radiology Departments worldwide. *Deep-learning* methods could obviate the complexity of the radiomic process, as the system processes all the information derived from the feature maps and should be catilizedngcognising a precise pattern and providing the final answer, similarly to what the human brain would do [16,37]: however, these neural networks are still far from perfect and are, in any case, dependent on the development of trustworthy ra-

diomic models. It is critical to remember that textural analysis, being based on pixel/voxel gray-level analysis, highly suffers from MR-based artifacts [37], and is influenced by the signal-to-noise ratio (SNR) and spatial resolution (which is already known to be lower in MR ttilizedmoreovoer, some variability dependintilized utilised software for texture analysis is expected, and that is another factor that shall be acquired for in future studies. Another potentially confounding factor may derive from the statistical processes applied to select the most significant features and avoid overfitting: among these methods are the so-called *regression tests* (e.g., LASSO) which aim to eliminate repetitive data, avoiding repetition and multicollinearity; however, they may involuntarily cause the loss of information, as the key to the neoplastic degeneration is the accumulation of multiple, repetitive mutations, which could somehow be depicted by the abundance of textural features. Of course, the argument is beyond the scope of the present paper, and we redirect the reader to a specific paper on statistics and mathematics.

We performed our analysis on T2w sequences (and not on DWI sequences or post-contrast imaging) because they are the core sequences of rectal cancer MR, so that our measurements are potentially reproducible in every setting; moreover, they are not as dependent as diffusion-weighted sequences on an algorithm's variation, although still reflecting the "pathologic" component inside the volume of study via their capability of reflecting the watery-content of tissues.

Radiomic and mathematical models are thoroughly gaining interest in the medical community, as they could support the clinicians' work in many ways, from the prediction of the response to CTRT to redrawing the patients' influx in the emergency department [39,43,44], thus allowing for the better allocation of the finite resources of the healthcare system worldwide.

5. Conclusions

To conclude, our study underlined the importance of preoperative texture analysis in discriminating responder and non-responder patients with advanced rectal cancer, with more than acceptable diagnostic values. Further studies should validate the presented result to enhance their application in clinical practice.

Author Contributions: Conceptualisation, D.I. and C.M.; methodology, D.I.; software, I.M.; validation, D.I.; formal analysis, I.M.; investigation, I.M., T.P.G., S.G.D. and C.T.F.; resources, C.M.; data curation, I.M.; writing—original draft preparation, C.M. and I.M.; writing—review and editing: all authors; visualisation: all authors; supervision, R.C., C.M. and P.N.F.; project administration, D.I.; funding acquisition, N/A. All authors have read and agreed to the published version of the manuscript.

Funding: This research received no external funding.

Institutional Review Board Statement: Ethical review and approval were waived for this study, due to its retrospective and anonymous nature.

Informed Consent Statement: Informed consent was obtained from all subjects involved in the study.

Data Availability Statement: The raw data supporting the conclusions of this article will be made available by the authors on request.

Conflicts of Interest: The authors declare no conflicts of interest.

References

1. Habr-Gama, A.; Perez, R.O.; Nadalin, W.; Sabbaga, J.; Ribeiro, U.; Silva E Sousa, A.H.; Campos, F.G.; Kiss, D.R.; Gama-Rodrigues, J. Operative Versus Nonoperative Treatment for Stage 0 Distal Rectal Cancer Following Chemoradiation Therapy: Long-Term Results. *Ann. Surg.* **2004**, *240*, 711–718. [CrossRef] [PubMed]
2. Santiago, I.; Rodrigues, B.; Barata, M.; Figueiredo, N.; Fernandez, L.; Galzerano, A.; Parés, O.; Matos, C. Re-Staging and Follow-up of Rectal Cancer Patients with MR Imaging When "Watch-and-Wait" Is an Option: A Practical Guide. *Insights Imaging* **2021**, *12*, 114. [CrossRef]
3. Habr-Gama, A.; Gama-Rodrigues, J.; São Julião, G.P.; Proscurshim, I.; Sabbagh, C.; Lynn, P.B.; Perez, R.O. Local Recurrence After Complete Clinical Response and Watch and Wait in Rectal Cancer After Neoadjuvant Chemoradiation: Impact of Salvage Therapy on Local Disease Control. *Int. J. Radiat. Oncol. Biol. Phys.* **2014**, *88*, 822–828. [CrossRef] [PubMed]

4. Arya, S.; Sen, S.; Engineer, R.; Saklani, A.; Pandey, T. Imaging and Management of Rectal Cancer. *Semin. Ultrasound CT MRI* **2020**, *41*, 183–206. [CrossRef]
5. Bernier, L.; Balyasnikova, S.; Tait, D.; Brown, G. Watch-and-Wait as a Therapeutic Strategy in Rectal Cancer. *Curr. Color. Cancer Rep* **2018**, *14*, 37–55. [CrossRef]
6. Benson, A.B.; Venook, A.P.; Al-Hawary, M.M.; Azad, N.; Chen, Y.-J.; Ciombor, K.K.; Cohen, S.; Cooper, H.S.; Deming, D.; Garrido-Laguna, I.; et al. Rectal Cancer, Version 2.2022, NCCN Clinical Practice Guidelines in Oncology. *J. Natl. Compr. Cancer Netw.* **2022**, *20*, 1139–1167. [CrossRef]
7. Lang, D.; Ciombor, K.K. Diagnosis and Management of Rectal Cancer in Patients Younger Than 50 Years: Rising Global Incidence and Unique Challenges. *J. Natl. Compr. Cancer Netw.* **2022**, *20*, 1169–1175. [CrossRef] [PubMed]
8. Glynne-Jones, R.; Wyrwicz, L.; Tiret, E.; Brown, G.; Rödel, C.; Cervantes, A.; Arnold, D. Rectal Cancer: ESMO Clinical Practice Guidelines for Diagnosis, Treatment and Follow-Up. *Ann. Oncol.* **2017**, *28*, iv22–iv40. [CrossRef]
9. Birlik, B.; Obuz, F.; Elibol, F.D.; Celik, A.O.; Sokmen, S.; Terzi, C.; Sagol, O.; Sarioglu, S.; Gorken, I.; Oztop, I. Diffusion-Weighted MRI and MR- Volumetry—In the Evaluation of Tumor Response after Preoperative Chemoradiotherapy in Patients with Locally Advanced Rectal Cancer. *Magn. Reson. Imaging* **2015**, *33*, 201–212. [CrossRef]
10. Barral, M.; Eveno, C.; Hoeffel, C.; Boudiaf, M.; Bazeries, P.; Foucher, R.; Pocard, M.; Dohan, A.; Soyer, P. Diffusion-Weighted Magnetic Resonance Imaging in Colorectal Cancer. *J. Visc. Surg.* **2016**, *153*, 361–369. [CrossRef]
11. Monguzzi, L.; Ippolito, D.; Bernasconi, D.P.; Trattenero, C.; Galimberti, S.; Sironi, S. Locally Advanced Rectal Cancer: Value of ADC Mapping in Prediction of Tumor Response to Radiochemotherapy. *Eur. J. Radiol.* **2013**, *82*, 234–240. [CrossRef] [PubMed]
12. Jhaveri, K.S.; Hosseini-Nik, H. MRI of Rectal Cancer: An Overview and Update on Recent Advances. *Am. J. Roentgenol.* **2015**, *205*, W42–W55. [CrossRef] [PubMed]
13. Cai, G. Diffusion-Weighted Magnetic Resonance Imaging for Predicting the Response of Rectal Cancer to Neoadjuvant Concurrent Chemoradiation. *WJG* **2013**, *19*, 5520. [CrossRef] [PubMed]
14. Sassen, S.; De Booij, M.; Sosef, M.; Berendsen, R.; Lammering, G.; Clarijs, R.; Bakker, M.; Beets-Tan, R.; Warmerdam, F.; Vliegen, R. Locally Advanced Rectal Cancer: Is Diffusion Weighted MRI Helpful for the Identification of Complete Responders (ypT0N0) after Neoadjuvant Chemoradiation Therapy? *Eur. Radiol.* **2013**, *23*, 3440–3449. [CrossRef]
15. Sun, Y.-S.; Zhang, X.-P.; Tang, L.; Ji, J.-F.; Gu, J.; Cai, Y.; Zhang, X.-Y. Locally Advanced Rectal Carcinoma Treated with Preoperative Chemotherapy and Radiation Therapy: Preliminary Analysis of Diffusion-Weighted MR Imaging for Early Detection of Tumor Histopathologic Downstaging. *Radiology* **2010**, *254*, 170–178. [CrossRef] [PubMed]
16. Coppola, F.; Giannini, V.; Gabelloni, M.; Panic, J.; Defeudis, A.; Lo Monaco, S.; Cattabriga, A.; Cocozza, M.A.; Pastore, L.V.; Polici, M.; et al. Radiomics and Magnetic Resonance Imaging of Rectal Cancer: From Engineering to Clinical Practice. *Diagnostics* **2021**, *11*, 756. [CrossRef]
17. Aerts, H.J.W.L.; Velazquez, E.R.; Leijenaar, R.T.H.; Parmar, C.; Grossmann, P.; Carvalho, S.; Bussink, J.; Monshouwer, R.; Haibe-Kains, B.; Rietveld, D.; et al. Decoding Tumour Phenotype by Noninvasive Imaging Using a Quantitative Radiomics Approach. *Nat. Commun.* **2014**, *5*, 4006. [CrossRef]
18. Mayerhoefer, M.E.; Materka, A.; Langs, G.; Häggström, I.; Szczypiński, P.; Gibbs, P.; Cook, G. Introduction to Radiomics. *J. Nucl. Med.* **2020**, *61*, 488–495. [CrossRef]
19. Tibermacine, H.; Rouanet, P.; Sbarra, M.; Forghani, R.; Reinhold, C.; Nougaret, S.; the GRECCAR Study Group; Rullier, E.; Lelong, B.; Maingon, P.; et al. Radiomics Modelling in Rectal Cancer to Predict Disease-Free Survival: Evaluation of Different Approaches. *Br. J. Surg.* **2021**, *108*, 1243–1250. [CrossRef]
20. Bibault, J.-E.; Giraud, P.; Housset, M.; Durdux, C.; Taieb, J.; Berger, A.; Coriat, R.; Chaussade, S.; Dousset, B.; Nordlinger, B.; et al. Deep Learning and Radiomics Predict Complete Response after Neo-Adjuvant Chemoradiation for Locally Advanced Rectal Cancer. *Sci. Rep.* **2018**, *8*, 12611. [CrossRef]
21. Bulens, P.; Couwenberg, A.; Intven, M.; Debucquoy, A.; Vandecaveye, V.; Van Cutsem, E.; D'Hoore, A.; Wolthuis, A.; Mukherjee, P.; Gevaert, O.; et al. Predicting the Tumor Response to Chemoradiotherapy for Rectal Cancer: Model Development and External Validation Using MRI Radiomics. *Radiother. Oncol.* **2020**, *142*, 246–252. [CrossRef] [PubMed]
22. Yip, S.S.F.; Aerts, H.J.W.L. Applications and Limitations of Radiomics. *Phys. Med. Biol.* **2016**, *61*, R150–R166. [CrossRef]
23. Van Timmeren, J.E.; Cester, D.; Tanadini-Lang, S.; Alkadhi, H.; Baessler, B. Radiomics in Medical Imaging—"How-to" Guide and Critical Reflection. *Insights Imaging* **2020**, *11*, 91. [CrossRef]
24. Rogers, W.; Thulasi Seetha, S.; Refaee, T.A.G.; Lieverse, R.I.Y.; Granzier, R.W.Y.; Ibrahim, A.; Keek, S.A.; Sanduleanu, S.; Primakov, S.P.; Beuque, M.P.L.; et al. Radiomics: From Qualitative to Quantitative Imaging. *Br. J. Radiol.* **2020**, *93*, 20190948. [CrossRef] [PubMed]
25. Stanzione, A.; Cuocolo, R.; Ugga, L.; Verde, F.; Romeo, V.; Brunetti, A.; Maurea, S. Oncologic Imaging and Radiomics: A Walkthrough Review of Methodological Challenges. *Cancers* **2022**, *14*, 4871. [CrossRef] [PubMed]
26. Beets-Tan, R.G.H.; Lambregts, D.M.J.; Maas, M.; Bipat, S.; Barbaro, B.; Curvo-Semedo, L.; Fenlon, H.M.; Gollub, M.J.; Gourtsoyianni, S.; Halligan, S.; et al. Magnetic Resonance Imaging for Clinical Management of Rectal Cancer: Updated Recommendations from the 2016 European Society of Gastrointestinal and Abdominal Radiology (ESGAR) Consensus Meeting. *Eur. Radiol.* **2018**, *28*, 1465–1475. [CrossRef]

27. Nioche, C.; Orlhac, F.; Boughdad, S.; Reuzé, S.; Goya-Outi, J.; Robert, C.; Pellot-Barakat, C.; Soussan, M.; Frouin, F.; Buvat, I. LIFEx: A Freeware for Radiomic Feature Calculation in Multimodality Imaging to Accelerate Advances in the Characterization of Tumor Heterogeneity. *Cancer Res.* **2018**, *78*, 4786–4789. [CrossRef]
28. Gillies, R.J.; Schabath, M.B. Radiomics Improves Cancer Screening and Early Detection. *Cancer Epidemiol. Biomark. Prev.* **2020**, *29*, 2556–2567. [CrossRef]
29. Horvat, N.; Veeraraghavan, H.; Nahas, C.S.R.; Bates, D.D.; Ferreira, F.R.; Zheng, J.; Capanu, M.; Fuqua, J.L.; Fernandes, M.C.; Sosa, R.E.; et al. Combined Artificial Intelligence and Radiologist Model for Predicting Rectal Cancer Treatment Response from Magnetic Resonance Imaging: An External Validation Study. *Abdom Radiol.* **2022**, *47*, 2770–2782. [CrossRef]
30. Cui, Y.; Yang, X.; Shi, Z.; Yang, Z.; Du, X.; Zhao, Z.; Cheng, X. Radiomics Analysis of Multiparametric MRI for Prediction of Pathological Complete Response to Neoadjuvant Chemoradiotherapy in Locally Advanced Rectal Cancer. *Eur. Radiol.* **2019**, *29*, 1211–1220. [CrossRef]
31. Staal, F.C.R.; van der Reijd, D.J.; Taghavi, M.; Lambregts, D.M.J.; Beets-Tan, R.G.H.; Maas, M. Radiomics for the Prediction of Treatment Outcome and Survival in Patients With Colorectal Cancer: A Systematic Review. *Clin. Color. Cancer* **2021**, *20*, 52–71. [CrossRef] [PubMed]
32. Shafiq-ul-Hassan, M.; Zhang, G.G.; Latifi, K.; Ullah, G.; Hunt, D.C.; Balagurunathan, Y.; Abdalah, M.A.; Schabath, M.B.; Goldgof, D.G.; Mackin, D.; et al. Intrinsic Dependencies of CT Radiomic Features on Voxel Size and Number of Gray Levels. *Med. Phys.* **2017**, *44*, 1050–1062. [CrossRef] [PubMed]
33. Park, S.-H.; Lim, H.; Bae, B.K.; Hahm, M.H.; Chong, G.O.; Jeong, S.Y.; Kim, J.-C. Robustness of Magnetic Resonance Radiomic Features to Pixel Size Resampling and Interpolation in Patients with Cervical Cancer. *Cancer Imaging* **2021**, *21*, 19. [CrossRef]
34. Espinasse, M.; Pitre-Champagnat, S.; Charmettant, B.; Bidault, F.; Volk, A.; Balleyguier, C.; Lassau, N.; Caramella, C. CT Texture Analysis Challenges: Influence of Acquisition and Reconstruction Parameters: A Comprehensive Review. *Diagnostics* **2020**, *10*, 258. [CrossRef] [PubMed]
35. Achilli, P.; Magistro, C.; Abd El Aziz, M.A.; Calini, G.; Bertoglio, C.L.; Ferrari, G.; Mari, G.; Maggioni, D.; Peros, G.; Tamburello, S.; et al. Modest Agreement between Magnetic Resonance and Pathological Tumor Regression after Neoadjuvant Therapy for Rectal Cancer in the Real World. *Int. J. Cancer* **2022**, *151*, 120–127. [CrossRef] [PubMed]
36. Crimì, F.; Valeggia, S.; Baffoni, L.; Stramare, R.; Lacognata, C.; Spolverato, G.; Albertoni, L.; Spimpolo, A.; Evangelista, L.; Zucchetta, P.; et al. [18F]FDG PET/MRI in Rectal Cancer. *Ann. Nucl. Med.* **2021**, *35*, 281–290. [CrossRef]
37. Lohmann, P.; Bousabarah, K.; Hoevels, M.; Treuer, H. Radiomics in Radiation Oncology—Basics, Methods, and Limitations. *Strahlenther Onkol.* **2020**, *196*, 848–855. [CrossRef]
38. Robins, M.; Solomon, J.; Hoye, J.; Abadi, E.; Marin, D.; Samei, E. Systematic Analysis of Bias and Variability of Texture Measurements in Computed Tomography. *J. Med. Imag.* **2019**, *6*, 033503. [CrossRef]
39. Shi, L.; Zhang, Y.; Hu, J.; Zhou, W.; Hu, X.; Cui, T.; Yue, N.J.; Sun, X.; Nie, K. Radiomics for the Prediction of Pathological Complete Response to Neoadjuvant Chemoradiation in Locally Advanced Rectal Cancer: A Prospective Observational Trial. *Bioengineering* **2023**, *10*, 634. [CrossRef]
40. Ng, F.; Kozarski, R.; Ganeshan, B.; Goh, V. Assessment of Tumor Heterogeneity by CT Texture Analysis: Can the Largest Cross-Sectional Area Be Used as an Alternative to Whole Tumor Analysis? *Eur. J. Radiol.* **2013**, *82*, 342–348. [CrossRef]
41. Rizzetto, F.; Calderoni, F.; De Mattia, C.; Defeudis, A.; Giannini, V.; Mazzetti, S.; Vassallo, L.; Ghezzi, S.; Sartore-Bianchi, A.; Marsoni, S.; et al. Impact of Inter-Reader Contouring Variability on Textural Radiomics of Colorectal Liver Metastases. *Eur Radiol Exp* **2020**, *4*, 62. [CrossRef] [PubMed]
42. Shen, C.; Liu, Z.; Guan, M.; Song, J.; Lian, Y.; Wang, S.; Tang, Z.; Dong, D.; Kong, L.; Wang, M.; et al. 2D and 3D CT Radiomics Features Prognostic Performance Comparison in Non-Small Cell Lung Cancer. *Transl. Oncol.* **2017**, *10*, 886–894. [CrossRef] [PubMed]
43. Mirmozaffari, M.; Kamal, N. The Application of Data Envelopment Analysis to Emergency Departments and Management of Emergency Conditions: A Narrative Review. *Healthcare* **2023**, *11*, 2541. [CrossRef] [PubMed]
44. Jovanovic, M.M.; Stefanovic, A.D.; Sarac, D.; Kovac, J.; Jankovic, A.; Saponjski, D.J.; Tadic, B.; Kostadinovic, M.; Veselinovic, M.; Sljukic, V.; et al. Possibility of Using Conventional Computed Tomography Features and Histogram Texture Analysis Parameters as Imaging Biomarkers for Preoperative Prediction of High-Risk Gastrointestinal Stromal Tumors of the Stomach. *Cancers* **2023**, *15*, 5840. [CrossRef]